

Robust Synthesis of Wind Turbine Generators to Support Microgrid Frequency Considering Linearization-Induced Uncertainty

Yichen Zhang, *Member, IEEE*, Chen Chen, *Senior Member, IEEE*, Tianqi Hong, *Member, IEEE*, Bai Cui, *Member, IEEE*, Bo Chen, *Member, IEEE*, Feng Qiu, *Senior Member, IEEE*

Abstract—The capability to switch between grid-connected and islanded modes has promoted adoption of microgrid technology for powering remote locations. Stabilizing frequency during the islanding event, however, is a challenging control task, particularly under high penetration of converter-interfaced sources. In this paper, a numerical optimal control (NOC)-based control synthesis methodology is proposed for preparedness of microgrid islanding that ensure guaranteed performance. The key feature of the proposed paradigm is near real-time centralized scheduling for real-time decentralized executing. For tractable computation, linearized models are used in the problem formulation. To accommodate the linearization errors, interval analysis is employed to compute linearization-induced uncertainty as numerical intervals so that the NOC problem can be formulated into a robust mixed-integer linear program. The proposed control is verified on the full nonlinear model in Simulink. The simulation results shown effectiveness of the proposed control paradigm and the necessity of considering linearization-induced uncertainty.

Index Terms—Microgrids, frequency response, wind turbine generator, uncertainty quantification, reachability, interval analysis, numerical optimal control, mixed-integer linear programming.

NOMENCLATURE

Mathematical Symbols

A, B, E State, control input, disturbance input matrices
 C, D, F Output, control feedforward, disturbance feedforward matrices
 Δ Deviation from operating point

Physical Variables

All variables are in per unit unless specified.

ψ Flux linkage
 v, i Instantaneous voltage, current
 R_s, L_l, L_m Resistance, leakage, mutual inductance
 $\vec{\Psi}_s, \Psi_s$ Space vector of stator flux and its magnitude
 \vec{V}_s, V_s Space vector of stator voltage and its magnitude
 H_D, H_T Diesel, wind turbine generator inertia constant [s]
 P_m, P_v Diesel generator mechanical power, valve position
 R Governor droop setting
 τ_d, τ_{sm} Diesel engine, governor time constant [s]

ω_c Cut-off frequency of low-pass filter [Hz]
 ω_d, ω_r Diesel, wind turbine angular speed
 ω_f^* Filtered reference speed for wind turbine generator
 ω_s Synchronous angular speed
 $\bar{\omega}$ Speed base of wind turbine generator [rad/s]
 \bar{f} Speed base of diesel generator [Hz]
 K^T Torque controller gain
 K^Q Reactive power controller gain
 K^C Current controller gain
 u_{ie} Supplementary input for model reference control

Subscripts and Superscripts
 d, q Direct, quadrature axis component
 s, r Stator, rotor
 P, I Proportional, integral
 p, r Physical plant, reference model
 $*$ Reference and command

I. INTRODUCTION

The capability to switch between grid-connected and islanded modes has promoted adoption of microgrid technology for powering remote locations [1] as well as improving grid resiliency [2]–[4]. The microgrids should be able to withstand islanding-induced perturbations and successfully establish frequency and voltage regulation [5], [6]. A strategy for reducing associated frequency and voltage deviations entails bringing power at the point of common coupling (PCC) to zero prior to disconnection [7]. Such a strategy, however, can only be applied for slower time-scale islanding, not for emergency ones. During emergency islanding, PCC power, as disturbance, is directly imposed on the microgrids, leading to frequency and voltage deviation, which should be maintained within permissible ranges as large excursion may trigger protection relays and make distributed energy resources (DERs) disconnected. Particularly, maintaining frequency within safe limits becomes more challenging under increasing penetration of renewable energy, which is the main reason of the inertia reduction in microgrids [8].

Various strategies have been proposed to tackle this challenge [9]–[13]. The particle swarm optimization (PSO) techniques to tune the proportional-integral (PI) based frequency controllers are presented in [9] so that the overshoot and oscillation of the frequency response can be reduced. Demonstration of using battery energy storage systems (BESSs) for frequency support is presented in [10]. The robust control

This work was supported by US DOE ARPA-E NODES program.

Y. Zhang, T. Hong, B. Chen and F. Qiu are with Argonne National Laboratory, Lemont, IL 60439 USA (email: yichen.zhang@anl.gov).

C. Chen is with Xi'an Jiaotong University, Xi'an, Shaanxi, 710049 China.

B. Cui is with National Renewable Energy Laboratory, Golden, CO 80401, USA.

approaches are applied to minimize battery size and reduce frequency variation simultaneously [11]. A multiple-time-scales hierarchical frequency stability control architecture is proposed in [12] to address the variability of renewable sources and load. The model reference control paradigm is employed in [13] to achieve programmable inertial response. The gaps, however, still exist in the following perspectives: (1) permissible limits are not enforced as pointed out by [8], (2) dynamics of the primary energy sources are over-simplified as mentioned by [14], (3) modeling errors, particularly linearization error, has not been rigorously analyzed and compensated.

Based on our previous work [15], a robust control paradigm for regulating microgrid frequency under emergent islanding events is proposed in this paper. This control system relies on local controllers to execute real-time commands and a central control system to coordinate multiple resources and adjust local controller parameters in near real-time. The objective is to compute feasible supplementary control signals for wind turbine generators (WTGs) [16], [17] so that the stored kinetic energy can be optimally used to support the frequency. The control is strategically configured as a two-level paradigm. The upper layer is a near real-time control scheduling module, which solves a numerical optimal control (NOC) problem to obtain supplementary control signals. The computation is performed once significant changes of system operating condition have been identified. To reduce the computation complex, linearized models are employed in the NOC problem, while linearization error is rigorously analyzed. Once the bounds of linearization-induced uncertainty is obtained, the NOC can be formulated as a robust mixed-integer linear program (MILP). The computed signals will be sent to the lower layer, whose responsibility is to monitor the islanding event and execute the signals upon islanding. Such a *near real-time centralized scheduling for real-time decentralized executing* structure has been employed by many researchers to solve challenging control tasks in power systems [15], [18], [19]. The contributions of this paper are briefly concluded:

- 1) We analyze the linearization error of WTG models, and obtain the bounds using interval analysis.
- 2) We formulate the near real-time NOC problem as a robust MILP, analyze the worst-case realization with a MILP re-formulation.
- 3) We propose and implement a novel control paradigm and verify its effectiveness using three-phase nonlinear simulation in Simulink.

The reminder of the paper is organized as follows. Section II discusses the frequency response in microgrids and derives the linearization-induced uncertainty. Section III details the control paradigm. Section IV presents the case studies, followed by conclusion in V.

1) *Notations*: Let $\dot{x} \in f(x)$ denotes differential inclusions. Let \oplus denotes Minkowski addition of two sets.

II. MICROGRID MODELS

Practically, microgrids are usually fed by mixed sources of diesel generators (DGs) and distributed energy resources (DERs) for reliability and cost effectiveness [1]. Among all

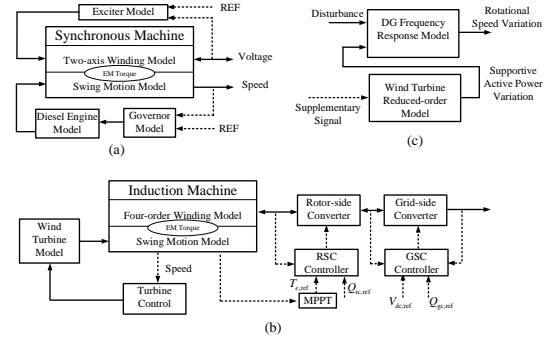


Fig. 1. (a) Modules and their interactions of diesel generation. (b) Modules and their interactions of wind turbine generator. (c) Augmented frequency response model.

DERs, WTGs are one of the fastest growing clean power sources. Therefore, DGs and WTGs are considered in this study. The modules of DG and WTG are shown in Fig. 1 (a) and (b), respectively. The main objective of this section is to derive the augmented frequency response (AFR) model illustrated in Fig. 1 (c), which describes the microgrid frequency dynamics (considered equivalent to the speed of DG) subjected to both disturbances and supports. Such models have been shown to be crucial for frequency studies [20]. Compared with the models in [13] and [15], we use full-order linearized WTG model instead, and express the linearization error as a unknown-but-bounded set.

A. Diesel Generator and Its Analytical Model

A diesel generator (DG) is a combustion engine driven synchronous generator. A complete model consists of a two-axis synchronous machine, combustion engine, governor, and exciter shown in Fig. 1 (a). The governor, engine, and swing dynamics shown in (1) are extracted to describe the frequency characteristics of the diesel generator, which has proved to be precise in many power system applications [20]

$$\begin{aligned} 2H_d \Delta \dot{\omega}_d &= \bar{f}(\Delta P_m - \Delta P_e) \\ \tau_d \Delta \dot{P}_m &= -\Delta P_m + \Delta P_v \\ \tau_g \Delta \dot{P}_v &= -\Delta P_v - \Delta \omega_d / (\bar{f} R_D) \end{aligned} \quad (1)$$

It is worth mentioning that the model in (1) can also present the frequency response of an aggregated group of DGs. Ref. [20] and [13] have shown such an aggregation is accurate, especially in microgrids due to the closer electric distance.

B. Double Fed Induction Generator (DFIG)-Based WTG and Its Analytical Model

The zero-axis DFIG-based WTG can be described using the following differential-algebraic equations

$$\dot{\omega}_r = 1/(2H_T)(T_m - T_e) \quad (2)$$

$$\dot{\omega}_f^* = \omega_c(\omega_r^* - \omega_f^*) \quad (3)$$

$$\dot{x}_1 = K_I^T(\omega_f^* - \omega_r + u_{ie}) \quad (4)$$

$$\dot{x}_2 = K_I^Q(Q_g^* - Q_g) \quad (5)$$

$$\dot{x}_3 = K_I^C(i_{qr}^* - i_{qr}) \quad (6)$$

$$\dot{x}_4 = K_I^C(i_{dr}^* - i_{dr}) \quad (7)$$

$$0 = \bar{\omega}(v_{qs} - R_s i_{qs} - \omega_s \psi_{ds}) \quad (8)$$

$$0 = \bar{\omega}(v_{ds} - R_s i_{ds} + \omega_s \psi_{qs}) \quad (9)$$

$$0 = \bar{\omega}[v_{qr} - R_r i_{qr} - (\omega_s - \omega_r) \psi_{dr}] \quad (10)$$

$$0 = \bar{\omega}[v_{dr} - R_r i_{dr} + (\omega_s - \omega_r) \psi_{qr}] \quad (11)$$

$$0 = -\psi_{qs} + L_s i_{qs} + L_m i_{qr} \quad (12)$$

$$0 = -\psi_{ds} + L_s i_{ds} + L_m i_{dr} \quad (13)$$

$$0 = -\psi_{qr} + L_r i_{qr} + L_m i_{qs} \quad (14)$$

$$0 = -\psi_{dr} + L_r i_{dr} + L_m i_{ds} \quad (15)$$

$$0 = P_g + (v_{qs} i_{qs} + v_{qs} i_{qs}) + (v_{qr} i_{qr} + v_{qr} i_{qr}) \quad (16)$$

$$0 = Q_g + (v_{qs} i_{ds} - v_{ds} i_{qs}) + (v_{qr} i_{dr} - v_{dr} i_{qr}) \quad (17)$$

$$0 = -v_{qr} + x_3 + K_P^C (i_{qr}^* - i_{qr}) + (\omega_s - \omega_r) (\sigma L_r i_{dr} + \frac{\Psi_s L_m}{L_s}) \quad (18)$$

$$0 = -v_{dr} + x_4 + K_P^C (i_{dr}^* - i_{dr}) - (\omega_s - \omega_r) \sigma L_r i_{qr} \quad (19)$$

Due to the page limit, detailed description is omitted here and can be found in [13].

C. Linearization Error and Induced Uncertainty

As we can see, the frequency response of DGs in (1) is originally linear, while the WTG model from (2) to (19) is nonlinear. To admit a MILP, linearization is taken, while the induced error is evaluated and expressed as a bounded uncertainty set. Let the overall WTG model in (2) – (19) expressed compactly as follows

$$\dot{x}_w = f(x_w, u_{sp}, y_w), \quad 0 = g(x_w, u_{sp}, y_w) \quad (20)$$

with the output equations

$$z = h(x_w, u_{sp}, y_w) \quad (21)$$

where

$$x_w = [\omega_r, \omega_f^*, x_1, x_2, x_3, x_4]^T, \quad z = [P_g]$$

$$y_w = [\psi_{qs}, \psi_{ds}, \psi_{qr}, \psi_{dr}, i_{qs}, i_{ds}, i_{qr}, i_{dr}, V_{qr}, V_{dr}, P_g, Q_g]^T$$

Let $s = [x_w, u_{sp}, y_w]$ and $s^{eq} = [x_w^{eq}, 0, y_w^{eq}]$ denote the equilibrium point. Using Taylor expansion at the equilibrium point x_w^{eq} and y_w^{eq} for the nonlinear DAEs yields

$$\begin{aligned} \dot{x}_w &\in f(s^{eq}) + A_{sys} \underbrace{(x_w - x_w^{eq})}_{\Delta x_w} + B_{sys} u_{sp} \\ &\quad + C_{sys} \underbrace{(y_w - y_w^{eq})}_{\Delta y_w} \oplus I(\xi) \end{aligned} \quad (22)$$

$$\begin{aligned} 0 &\in \underbrace{g(s^{eq})}_{=0} + D_{sys} \underbrace{(x_w - x_w^{eq})}_{\Delta x_w} + E_{sys} u_{sp} \\ &\quad + F_{sys} \underbrace{(y_w - y_w^{eq})}_{\Delta y_w} \oplus J(\xi) \end{aligned} \quad (23)$$

$$\begin{aligned} z &\in h(s^{eq}) + L_{sys} \underbrace{(x_w - x_w^{eq})}_{\Delta x_w} + M_{sys} u_{sp} \\ &\quad + N_{sys} \underbrace{(y_w - y_w^{eq})}_{\Delta y_w} \oplus K(\xi) \end{aligned} \quad (24)$$

where $I(\xi)$, $J(\xi)$ and $K(\xi)$ are the Lagrangian remainders. The i th row of $I(\xi)$, $J(\xi)$ and $K(\xi)$, denoted as $I_i(\xi)$, $J_i(\xi)$ and $K_i(\xi)$, respectively, reads

$$\begin{aligned} I_i(\xi) &= \frac{1}{2} (s - s^{eq})^T H_i^d(\xi) (s - s^{eq}) \\ J_i(\xi) &= \frac{1}{2} (s - s^{eq})^T H_i^a(\xi) (s - s^{eq}) \\ K_i(\xi) &= \frac{1}{2} (s - s^{eq})^T H_i^o(\xi) (s - s^{eq}) \end{aligned} \quad (25)$$

where H_i^d , H_i^a and H_i^o are the Hessian matrices for the i th row of the differential equation f_i , algebraic equation g_i , and output equation h_i . Lagrangian remainders enclose all higher-order terms if ξ can take any value of the linear combination of s and s^{eq}

$$\xi \in \{\alpha s + (1 - \alpha) s^{eq} | \alpha \in [0, 1]\} \quad (26)$$

For index-1 DAEs, the algebraic variables can be expressed in terms of differential and control variables as follows

$$\begin{aligned} (y_w - y_w^{eq}) &\in -F_{sys}^{-1} D_{sys} (x_w - x_w^{eq}) \\ &\quad - F_{sys}^{-1} E_{sys} u_{sp} \oplus [-F_{sys}^{-1} J(\xi)] \end{aligned} \quad (27)$$

Then, the differential equations read

$$\begin{aligned} \dot{x}_w &\in f(s^{eq}) + [A_{sys} - C_{sys} F_{sys}^{-1} D_{sys}] (x_w - x_w^{eq}) \\ &\quad + [B_{sys} - C_{sys} F_{sys}^{-1} E_{sys}] u_{sp} \\ &\quad \oplus I(\xi) \oplus [-C_{sys} F_{sys}^{-1} J(\xi)] \end{aligned} \quad (28)$$

And, the output equations can be re-written as follows

$$\begin{aligned} z &\in h(s^{eq}) + [L_{sys} - N_{sys} F_{sys}^{-1} D_{sys}] (x_w - x_w^{eq}) \\ &\quad + [M_{sys} - N_{sys} F_{sys}^{-1} E_{sys}] u_{sp} \\ &\quad \oplus K(\xi) \oplus [-C_{sys} F_{sys}^{-1} J(\xi)] \end{aligned} \quad (29)$$

Then, the equations expressed in terms of the deviation variables are expressed as follows

$$\begin{aligned} \Delta \dot{x}_w &\in \underbrace{[A_{sys} - C_{sys} F_{sys}^{-1} D_{sys}]}_{A_w} \Delta x_w \\ &\quad + \underbrace{[B_{sys} - C_{sys} F_{sys}^{-1} E_{sys}]}_{B_w} u_{sp} \\ &\quad \oplus I(\xi) \oplus [-C_{sys} F_{sys}^{-1} J(\xi)] \end{aligned} \quad (30)$$

$$\begin{aligned} \Delta z &\in \underbrace{[L_{sys} - N_{sys} F_{sys}^{-1} D_{sys}]}_{C_w} \Delta x_w \\ &\quad + \underbrace{[M_{sys} - N_{sys} F_{sys}^{-1} E_{sys}]}_{D_w} u_{sp} \\ &\quad \oplus K(\xi) \oplus [-C_{sys} F_{sys}^{-1} J(\xi)] \end{aligned} \quad (31)$$

which can be simplified as follows

$$\begin{aligned} \Delta \dot{x}_w &\in A_w \Delta x_w + B_w u_{sp} \oplus \underbrace{I(\xi) \oplus [-C_{sys} F_{sys}^{-1} J(\xi)]}_{S(\xi, s)} \\ \Delta z &\in C_w \Delta x_w + D_w u_{sp} \oplus \underbrace{K(\xi) \oplus [-N_{sys} F_{sys}^{-1} J(\xi)]}_{O(\xi, s)} \end{aligned} \quad (32)$$

where the terms $S(\xi, s)$ and $O(\xi, s)$ bound the linearization errors.

D. Numerical Evaluation of Linearization Errors

The linearization error terms $S(\xi, s)$ and $O(\xi, s)$ are complicated functions of several differential and algebraic variables besides the control inputs. It is extremely difficult to directly incorporate these term in the optimization model analytically, and numerical methods are indispensable. Thus, we will first evaluate their numerical intervals, and incorporate them as the unknown-but-bounded uncertainty sets into the optimization. The subsection will describe essential steps to obtain the numerical intervals.

The first step is to enclose ξ and s in intervals. This can be done by first computing the reachable sets of (20). With the time scale of interests, we can assume that the variations are caused only by the grid supportive control signals. Therefore, the over-approximation of the reachable sets can be performed if we bound the control input as \mathcal{U} , where $u_{sp} \in \mathcal{U}$. In turn, this control bound \mathcal{U} will be enforced in the NOC. The over-approximation algorithms propagate the set-represented inputs and initial condition under the system vector fields efficiently. The efficiency relies on the special representations of sets as boxes, ellipsoids, polytopes, support functions and so on [21]. Among all representations, the zonotopes [22], a sub-class of polytopes, has been widely-used since they are closed under linear transformation and Minkowski sum. The zonotope-based reachability computation has been applied to linear systems [23], [24], nonlinear systems [25], and nonlinear differential-algebraic systems [26]. Then, the obtained reachable sets, which are typically high-order zonotopes and difficult for general computational operations, will be converted into intervals by certain interval hull over-approximation methods. Detailed description of the algorithms is out of scope of this paper, and can be found in [22]–[26]. In this paper, we employ the zonotope-based reachability analysis, and perform the computation using the Matlab toolbox CORA [26]. Eq. (26) indicates that ξ and s can be enclosed in the same interval. Let this interval be denoted as Θ , where $s, \xi \in \Theta$.

The second step is to conduct the bound evaluation for functions $S(\xi, s)$ and $O(\xi, s)$ subjected to the interval inputs s and ξ , where $s, \xi \in \Theta$. This problem can be formulated as two nonlinear optimization problems. However, the results could be local optimum, and fail the enclosure. Other approaches such as Monte-Carlo sampling are subjected to the similar flaw. On the other hand, the interval arithmetics, or interval analysis, aims to define a systematic rule of operations for intervals, interval vectors and matrices such that the exact solutions are always included [27]. Therefore, we will employ the interval arithmetics to calculate the interval of $S(\xi, s)$ and $O(\xi, s)$, denoted as \mathcal{S} and \mathcal{O} , respectively. Thereto, we first compute the intervals of every element in the Hessian matrices $H_i^d(\xi)$, $H_i^a(\xi)$ and $H_i^o(\xi)$ to form the interval Hessian matrices \mathcal{H}_i^d , \mathcal{H}_i^a and \mathcal{H}_i^o , where the possible values of Hessian matrices are enclosed. Then, based on the results from the first step, we can express the term $\delta = s - s^{eq}$ as an interval vector, where $s \in \Theta$. Performing the interval multiplication between the interval vector δ and the interval Hessian matrices yields

the interval vectors of the Lagrangian remainders

$$\begin{aligned}\mathcal{I}_i &= [\underline{I}_i, \bar{I}_i] = \frac{1}{2} \delta^T \mathcal{H}_i^d \delta \\ \mathcal{J}_i &= [\underline{J}_i, \bar{J}_i] = \frac{1}{2} \delta^T \mathcal{H}_i^a \delta \\ \mathcal{K}_i &= [\underline{K}_i, \bar{K}_i] = \frac{1}{2} \delta^T \mathcal{H}_i^o \delta\end{aligned}\quad (33)$$

where \underline{I}_i and \bar{I}_i represent the upper and lower bound of $I_i(\xi)$ for $\xi \in \Theta$, and the same notation is applied for $J_i(\xi)$ and $K_i(\xi)$ as well. At last, the interval representations of the linearization errors can be calculated as follows

$$\begin{aligned}\mathcal{S} &= \mathcal{I} - C_{\text{sys}} F_{\text{sys}}^{-1} \mathcal{J} \\ \mathcal{O} &= \mathcal{K} - N_{\text{sys}} F_{\text{sys}}^{-1} \mathcal{J}\end{aligned}\quad (34)$$

Note that computations in (33) and (34) are interval operations defined in [27]. Such computations can be performed either by CORA [26] or a more fundamental Matlab toolbox INTLAB [28].

III. ROBUST NUMERICAL OPTIMAL CONTROL SYNTHESIS

A. Overall Configuration

The overall configuration of the proposed control is illustrated in Fig. 2. This control paradigm admits two essential features: near real-time scheduling (choosing policy) with real-time monitoring and control (choosing action), and centralized optimization with decentralized execution. Such strategies have been proved to be effective for controlling large-scale systems with *performance guarantees* [15], [18], [19].

The control paradigm is configured into two levels, that is, the centralized scheduling level and the decentralized triggering level. In the scheduling level, the grid operating status is acquired to update the parameters of the optimization model, including model parameters, linearization errors and PCC power. The linearization error analysis will be re-performed if the original operating points of WTGs change. A threshold for the grid-supportive mode activation is considered to accommodate the responding time and communication delay of the islanding detection signal. Based on current PCC power, this threshold will be converted into the initial condition of the AFR model, which will also be passed to the optimization problem. With up-to-date information, the signal scheduling problem, which is formulated as a MILP, can be promptly solved by off-the-shelf commercial solvers.

The triggering level is configured locally at each WTG. The obtained supportive signals for WTGs are transmitted to the designated WTG to configure local control. The local threshold is also updated accordingly. Once the supportive function is determined to be activated, a local clock is activated so that the scheduled signals are synchronized with the real time. And the synchronized signals are applied to the supplementary loop of the WTGs.

B. Numerical Optimal Control for Scheduling Level

The AFR model can be obtained by integrating the WTG model in (32) with the frequency response model of DG in (1) as illustrated in Fig. 1 (c). Without loss of generality, we

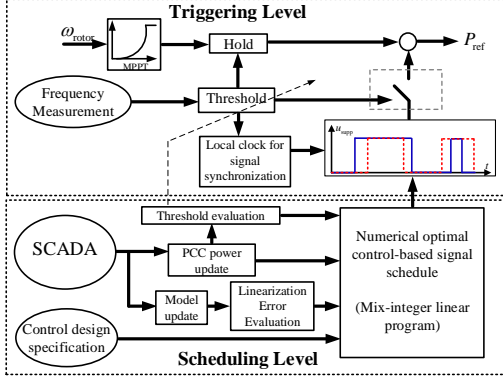


Fig. 2. Overall configuration of synthesizing performance guaranteed controller.

consider a microgrid with one DG and multiple WTGs. The term N_w is the number of WTGs, and \mathcal{N}_w is the set of WTG indices. Let S_d and $S_{w,i}$ be the base of DG and WTG i , respectively, and, $k_d = 1/S_d$, $k_{dw,i} = S_{w,i}/S_d$. It is very important to note that the uncertainty is introduced only when the WTG is activated for the grid supportive mode. Therefore, we introduce the binary variable b_i to indicate the activation status of WTG i , that is, b_i equals to one when the grid-supportive mode is on and zero otherwise. With all the above definition, the AFR can be expressed as follows

$$\begin{aligned} 2H_d\Delta\dot{\omega}_d &\in \bar{f}(\Delta P_m - k_d P_{\text{pcc}} + \sum_{i=1}^{N_w} k_{dw,i} \Delta P_{g,i}) \\ \tau_d \Delta \dot{P}_m &\in -\Delta P_m + \Delta P_v \\ \tau_g \Delta \dot{P}_v &\in -\Delta P_v - \Delta\omega_d / (\bar{f} R_D) \\ \Delta \dot{x}_{w,i} &\in A_{w,i} \Delta x_{w,i} + B_{w,i} u_{s,i} \oplus b_i \mathcal{O}_i \quad i \in \mathcal{N}_w \end{aligned} \quad (35)$$

where

$$\Delta P_{g,i} \in C_{w,i} \Delta x_{w,i} + D_{w,i} u_{s,i} \oplus b_i \mathcal{O}_i \quad i \in \mathcal{N}_w \quad (36)$$

where P_{pcc} is the current measured power flow at PCC. To obtain the overall state-space model, we first define the state and input vectors as follows

$$\begin{aligned} x &= [\Delta\omega_d, \Delta P_m, \Delta P_v, \Delta x_{w,1}, \dots, \Delta x_{w,i}, \dots, \Delta x_{w,N_w}]^T \\ u &= [u_{\text{sp},1}, \dots, u_{\text{sp},i}, \dots, u_{\text{sp},N_w}]^T \\ b &= [b_1, \dots, b_i, \dots, b_{N_w}]^T \\ \mathcal{S} &= [\mathcal{S}_1^T, \dots, \mathcal{S}_i^T, \dots, \mathcal{S}_{N_w}^T]^T \\ \mathcal{O} &= [\mathcal{O}_1, \dots, \mathcal{O}_i, \dots, \mathcal{O}_{N_w}^T]^T \end{aligned}$$

Then, substituting (36) into (35) yields the following state-space model

$$\dot{x} \in Ax + B_1 u + B_2 k_d P_{\text{pcc}} \oplus B_3 (b \circ \mathcal{S}) \oplus B_4 (b \circ \mathcal{O}) \quad (37)$$

where \circ denotes the Hadamard product, which performs the element-wise multiplication of two matrices with the same dimensions. The analytical model in (37) is discretized at a sample time of t_s and expressed compactly as follows

$$\begin{aligned} x(k+1) &\in A_d x(k) + B_{d1} u(k) + B_{d2} k_d P_{\text{pcc}} \\ &\oplus B_{d3} [b(k) \circ \mathcal{S}(k)] \oplus B_{d4} [b(k) \circ \mathcal{O}(k)] \end{aligned} \quad (38)$$

Let $\mathcal{T} = [0, 1, \dots, T]$ be the discretized time series of the overall scheduling horizon, $k \in \mathcal{Z} = [1, 2, \dots, Z]$ be its indices, and $\Gamma(\bullet) : \mathbb{R} \mapsto \mathbb{Z}$ be the mapping from the time series to the indices. First, the frequency deviation, that is, the rotor speed of the DG, should not exceed a certain limit in any time, that is,

$$\Delta\omega_d(k) \leq \Delta f_{d,\text{lim}} \quad \forall k \in \mathcal{Z} \quad (39)$$

No absolute value is used since the reverse power flow at PCC is excluded based on real practice. Since the kinetic energy of WTGs will be transferred to active power to support the grid, the speed of WTGs will decrease from nominal values. This deviation is also desired to be limited for all WTGs

$$|\Delta\omega_{r,i}(k)| \leq \Delta f_{w,\text{lim}} \quad \forall k \in \mathcal{Z}, i \in \mathcal{N}_w \quad (40)$$

For the ease of implementation, we confine the control signal to be the multi-level step function. Therefore, the control inputs are subjected to the following constraints

$$\begin{aligned} u_{s,i}(k) &= u_i(k) u_L \quad \forall k \in \mathcal{Z}, i \in \mathcal{N}_w \\ 0 &\leq u_i(k) \leq u_{\text{BD}} \quad \forall k \in \mathcal{Z}, i \in \mathcal{N}_w \end{aligned} \quad (41)$$

where u_i is an integer variable indicating the power level of the grid-supportive mode of WTG i , u_L is the fixed magnitude of one-level input, and u_{BD} is the total number of power levels. In addition, for the sake of efficiency, we would like to limit the number of times that one WTG is activated for grid support. Thereto, we first build up the constraint between $b_i(k)$ and $u_i(k)$, that is, $b_i(k)$ equals to one if $u_i(k) > 0$ and zero if $u_i(k) = 0$. This logic relation is expressed by the following constraints

$$0 \leq -u_i(k) + M b_i(k) \leq M - 1 \quad \forall k \in \mathcal{Z}, i \in \mathcal{N}_w \quad (42)$$

where M is a big positive number. Then, another binary variable $v_i(k)$ is defined to indicate the grid-supportive mode change from off to on of the WTG i by enforcing $v_i(k)$ to be one if the grid-supportive mode of WTG i is activated at time step k and zero otherwise using the following constraint

$$v_i(k) \geq b_i(k) - b_i(k-1) \quad \forall k = 2, \dots, Z, i \in \mathcal{N}_w \quad (43)$$

Obviously, $v_i(k)$ will be enforced to equal to one if the grid-supportive mode of WTG i is off at step $k-1$ and activated at step k . Otherwise, $v_i(k)$ could be either zero or one. Therefore, we impose the following constraints to limit the activation times of a WTG no more than two times during one event

$$\sum_{k=1}^Z v_i(k) \leq 2 \quad \forall i \in \mathcal{N}_w \quad (44)$$

The grid-supportive mode of all WTGs should be off at the beginning and end of the scheduling horizon

$$u_i(0) = 0, u_i(Z) = 0 \quad \forall i \in \mathcal{N}_w \quad (45)$$

Considering the threshold, the NOC should start from a designate initial condition instead of zero

$$x(0) = X_0 \quad (46)$$

The objective is to minimize the control efforts. The total control effort can be represented as the summation of all integer variables as

$$C_U = \sum_{i=1}^{N_w} \sum_{k=1}^T u_i(k) \quad (47)$$

The scheduling problem can be summarized as follows

$$\begin{aligned} \min \quad & C_U = \sum_{i=1}^{N_w} \sum_{k=1}^T u_i(k) \\ \text{s.t.} \quad & x(0) = X_0 \\ & x(k+1) \in A_d x(k) + B_{d1} u(k) + B_{d2} k_d P_{\text{pcc}} \\ & \quad \oplus B_{d3} [b(k) \circ \mathcal{S}(k)] \oplus B_{d4} [b(k) \circ \mathcal{O}(k)] \\ & \Delta \omega_d(k) \leq \Delta f_{d,\text{lim}} \quad \forall k \in \mathcal{Z} \\ & |\Delta \omega_{r,i}(k)| \leq \Delta f_{w,\text{lim}} \quad \forall k \in \mathcal{Z}, i \in \mathcal{N}_w \\ & u_{s,i}(k) = u_i(k) u_L \quad \forall k \in \mathcal{Z}, i \in \mathcal{N}_w \\ & 0 \leq u_i(k) \leq u_{\text{BD}} \quad \forall k \in \mathcal{Z}, i \in \mathcal{N}_w \\ & 0 \leq -u_i(k) + M b_i(k) \leq M - 1 \quad \forall k \in \mathcal{Z}, i \in \mathcal{N}_w \\ & \sum_{k=1}^Z v_i(k) \leq 2 \quad \forall i \in \mathcal{N}_w \\ & u_i(0) = 0, u_i(Z) = 0 \quad \forall i \in \mathcal{N}_w \end{aligned} \quad (48)$$

C. Robust Optimization Re-formulation

Note that problem (48) is infinite dimensional due to the uncertainty set. The formulation involving the uncertainty sets needs to be re-formulated so that the worst-case realization of the uncertainty can be revealed. Since the robust sets are interval and the problem is MILP, the standard re-formulation method in [29]–[31] can be employed. Particularly, dynamic systems with input uncertainty has been considered in [30], [31].

Let a realization of the uncertainty $\mathcal{S}(k)$ and $\mathcal{O}(k)$ be denoted as $\tilde{s}(k)$ and $\tilde{o}(k)$, respectively. Then, the differential inclusion in (38) can be expressed as

$$\begin{aligned} x(k+1) = & A_d x(k) + B_{d1} u(k) + B_{d2} k_d P_{\text{pcc}} \\ & + B_{d3} [b(k) \circ \tilde{s}(k)] + B_{d4} [b(k) \circ \tilde{o}(k)] \end{aligned} \quad (49)$$

The constraints on evolution discrete-time dynamics can be expressed in a compact notation as

$$\mathbf{x} = \mathcal{A}x(0) + \mathcal{B}_{d1}\mathbf{u} + \mathcal{B}_{d2}k_d P_{\text{pcc}} + \mathcal{B}_{d3}\mathbf{s} + \mathcal{B}_{d4}\mathbf{o} \quad (50)$$

where

$$\begin{aligned} \mathbf{x} &= [x(1), x(2), \dots, x(Z)]^T, \mathbf{u} = [u(0), u(1), \dots, u(Z-1)]^T \\ \mathbf{s} &= [b(0) \circ \tilde{s}(0), b(1) \circ \tilde{s}(1), \dots, b(Z-1) \circ \tilde{s}(Z-1)]^T \\ \mathbf{o} &= [b(0) \circ \tilde{o}(0), b(1) \circ \tilde{o}(1), \dots, b(Z-1) \circ \tilde{o}(Z-1)]^T \end{aligned}$$

$$\mathcal{A} = \begin{bmatrix} A \\ A^2 \\ \vdots \\ A^N \end{bmatrix} \quad \mathcal{B}_{di} = \begin{bmatrix} B_{di} & 0 & \cdots & 0 \\ AB_{di} & B_{di} & \cdots & 0 \\ \vdots & \vdots & \ddots & \vdots \\ A^{N-1}B_{di} & A^{N-2}B_{di} & \cdots & B_{di} \end{bmatrix}$$

where i denotes the different subscripts of the input matrices. Substituting (50) into constraint (39) yields

$$-Ax(0) - \mathcal{B}_{d1}\mathbf{u} - \mathcal{B}_{d2}k_d P_{\text{pcc}} - \mathcal{B}_{d3}\mathbf{s} - \mathcal{B}_{d4}\mathbf{o} \leq E\Delta f_{d,\text{lim}}$$

where E will ensure the constraint to be effective at appropriate rows. By grouping all uncertainty sets on the left-hand side we have

$$-\mathcal{B}_{d3}\mathbf{s} - \mathcal{B}_{d4}\mathbf{o} \leq E\Delta f_{d,\text{lim}} + Ax(0) + \mathcal{B}_{d1}\mathbf{u} + \mathcal{B}_{d2}k_d P_{\text{pcc}} \quad (51)$$

The robust constraint sanctification of (51) can be formulated as [31]

$$\begin{aligned} \max_w \quad & (-\mathcal{B}_{d3}\mathbf{s} - \mathcal{B}_{d4}\mathbf{o}) \leq E\Delta f_{d,\text{lim}} \\ & + Ax(0) + \mathcal{B}_{d1}\mathbf{u} + \mathcal{B}_{d2}k_d P_{\text{pcc}} \end{aligned} \quad (52)$$

Due to the special form of the uncertainty set, that is, interval, the worst-case realization can be revealed row-wise by determining the positivity of the entry of matrices \mathcal{B}_{d3} and \mathcal{B}_{d4} , which will depend on the system dynamic models.

IV. CASE STUDY

A. Enclosing Linearization Error

In this subsection, we will demonstrate the results of the analysis presented in Section II-D. As a prerequisite for the interval analysis, reachability analysis of the WTG in (2)-(19) is performed using CORA [26] under a bounded control input $\mathcal{U} = [0, 0.1]$, which will be enforced in the NOC. The reachable sets are shown in Fig. 3 in the format of zonotopes, which are further converted into intervals Θ . Then, the computations in (33) and (34) are performed to obtain the linearization error bounds in the format of intervals as follows

$$\mathcal{S} = \begin{bmatrix} [-0.001192776663658, 0.001190937295999] \\ [-0.000098120800673, 0.000098003228640] \\ [0, 0] \\ [-0.056868144117605, 0.056840867582327] \\ [-0.052150975958212, 0.052152050866097] \\ [-0.104503795886190, 0.104504716861513] \end{bmatrix}$$

$$\mathcal{O} = [[-0.024807136679364, 0.024828861362883]]$$

To further verify the bounds, reachability analysis of the linearized WTG in (32) under the inputs of a constant supplementary signal u_{sp} and error sets \mathcal{S} and \mathcal{O} . Simulated trajectory using the nonlinear model (2)-(19) under the same u_{sp} is compared in Fig. 4. With the obtained bounds, reachable sets of the linear system always enclose the trajectory of the nonlinear system. Note that the simulated nonlinear trajectories have been subtracted by the equilibrium points.

B. Frequency Control During Islanding

The optimization problem (48) can be converted into a MILP after applying the technique in Section III-C. The problem is formulated in the Yalmip environment [32] and solved by efficient solvers Gurobi. The parameters in the MILP are given as follows

$$\begin{aligned} t_s &= 0.1 \text{ [s]}, T = 10 \text{ [s]}, u_L = 0.02, u_{\text{BD}} = 5 \\ \Delta f_{d,\text{lim}} &= 0.5 \text{ [Hz]}, \Delta f_{w,\text{lim}} = 2 \text{ [Hz]} \end{aligned}$$

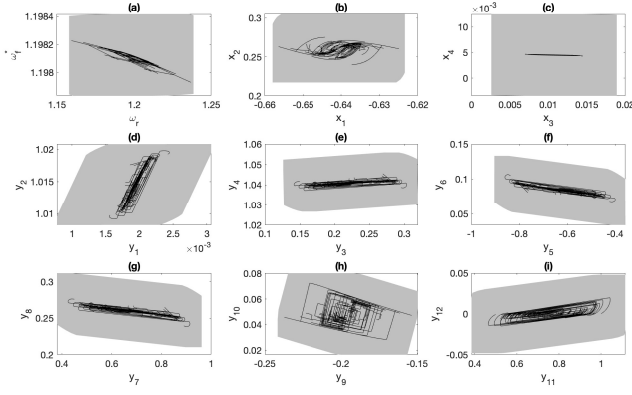


Fig. 3. Reachable sets of nonlinear WTG model under bounded input.

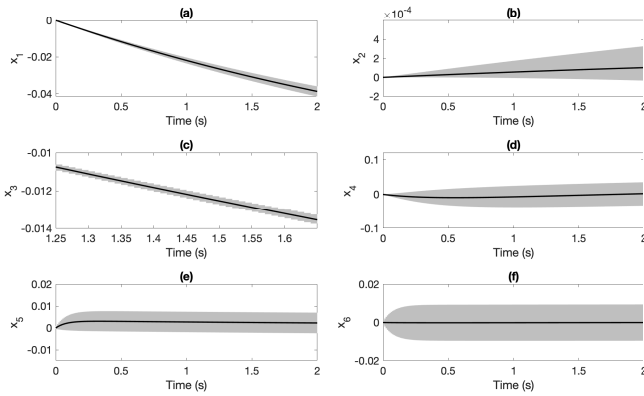


Fig. 4. Enclosing nonlinear trajectories by linear WTG with linearization error intervals.

Based on the given parameters, it is required that the frequency deviation to be limited within 0.5 Hz.

The microgrid model for verification is a modified 33-node three-phase built in Simulink environment illustrated in 5. All components shown in Fig. 1 have been implemented. Once the control signals are computed, they are set in the Simulink environment. Cascade-connected switches are employed to realized the control signal, the input magnitude and switching time of which will be adjusted accordingly. We

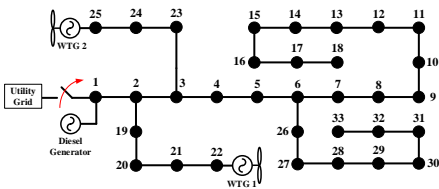


Fig. 5. Modified 33-node microgrid with diesel and wind turbine generators.

consider a scenario where the measured PCC power is 0.7 MW, and 0.14 per unit with respect to the DG. We assume the islanding detection and corresponding signal transmission can be completed within 0.1 second, which leads to an initial condition $X_0 = [-0.11, 0, 0, 0, \dots, 0]^T$ under current PCC power. After completing the up-to-date information process, the problem (48) is solved less than 10 seconds. The result is

plotted in Fig. 6 (a). The NOC problem without considering uncertainty is also solved and plotted in 6 (b). The total control effort C_U with the presence of the uncertainty is 42, while without considering uncertainty is 33. In addition, since the uncertainty is only presented when the WTG is activated for grid support, the control signals tend to attain their maximum values. In the latter case, though the grid-supportive mode activation duration is approximately the same, the signals are not reaching to their output limits in most of the activation duration.

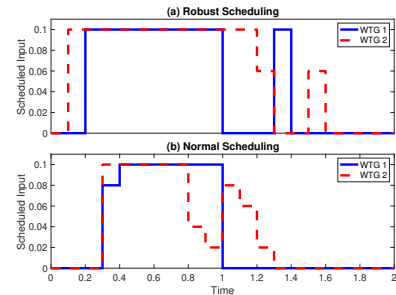


Fig. 6. Modified 33-node microgrid with diesel and wind turbine generators.

The computed signals are then equipped in the full-order three-phase nonlinear Simulink model for verification. We disconnect the switch at PCC to simulate the islanding event. Once the three state deviations of the DG cross the threshold X_0 , the grid-supportive mode is activated. The frequency responses of DG under no support, normally scheduled support and robustly scheduled support are shown in Fig. 7. The active power of the network is shown in Fig. 8. The previous two cases do not lead to safe responses, while the frequency in the last case stays within the permissible limits. In addition, the normally scheduled control is also applied to the linear system in Eq. (49) without considering the uncertainty, and the response is shown in Fig. 7 for comparison. As we can see, this response is safe but leaving no extra margins since the control effort is to be minimized. Therefore, if the linearization error of WTGs is not taken into account, the frequency response loses its safety. The active power variations of WTG 1 from linear and full nonlinear models are shown in Fig. 9.

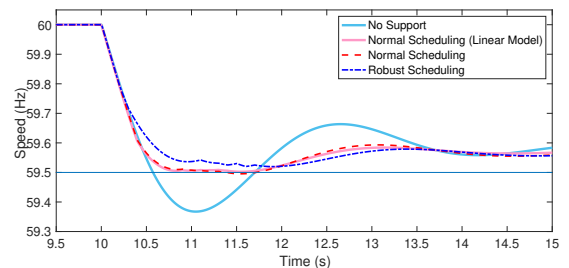


Fig. 7. Frequencies of DG under different cases.

V. CONCLUSIONS AND FUTURE WORKS

In this paper, a NOC-based control synthesis methodology is proposed for preparedness of microgrid islanding that can

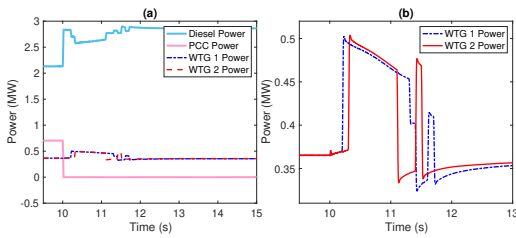


Fig. 8. (a) Active power in the network. (b) Enlarged view of WTG power.

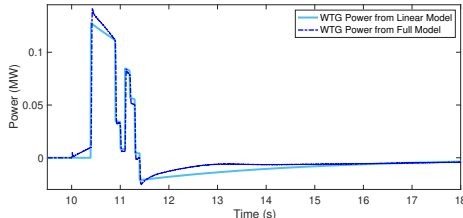


Fig. 9. Active power variations of WTGs from the linearized and full nonlinear model.

take the trajectory constraints, i.e., frequency response in this paper, into account. The key feature of the proposed paradigm is near real-time centralized scheduling for real-time decentralized executing. The controller schedules ahead a series of control signals to synthesize the grid-supportive mode of WTGs by solving the NOC problem, where the frequency response predicted by the AFR model satisfies the defined specifications under the current PCC power. Then, the computed signals are transmitted to individual WTGs for local activation. Linearization-induced uncertainty of WTGs is derived and computed using interval analysis. The proposed control is verified on the full nonlinear model in Simulink. The simulation results indicate the scheduling control can successfully retain the frequency within permissible ranges under the islanding event. Particularly, case studies show that considering uncertainty can create extra safety margins for accommodating modeling errors, and reserve safe responses. On the other hand, unsafe trajectory occurs if the uncertainty is omitted.

REFERENCES

- [1] R. Allen, D. Brutkoski, D. Farnsworth, and P. Larsen, "Sustainable energy solutions for rural alaska," Lawrence Berkeley Nat. Lab., Berkeley, CA, USA, Tech. Rep. LBNL-1005097, 2016.
- [2] C. Chen, J. Wang, F. Qiu, and D. Zhao, "Resilient distribution system by microgrids formation after natural disasters," *IEEE Trans. Smart Grid*, vol. 7, no. 2, pp. 958–966, 2016.
- [3] Z. Wang and J. Wang, "Self-healing resilient distribution systems based on sectionalization into microgrids," *IEEE Trans. Power Syst.*, vol. 30, no. 6, pp. 3139–3149, 2015.
- [4] J. Liu, X. Lu, and J. Wang, "Resilience analysis of DC microgrids under denial of service threats," *IEEE Trans. Power Syst.*, vol. 34, no. 4, pp. 3199–3208, 2019.
- [5] Y. Xu, H. Li, and L. M. Tolbert, "Inverter-based microgrid control and stable islanding transition," *2012 IEEE Energy Convers. Congr. Expo. ECCE 2012*, pp. 2374–2380, 2012.
- [6] X. Chen, J. Zhou, M. Shi, L. Yan, W. Zuo, and J. Wen, "A Novel virtual resistor and capacitor droop control for HESS in medium-voltage DC system," *IEEE Trans. Power Syst.*, vol. 34, no. 4, pp. 2518–2527, 2019.
- [7] S. A. R. Konakalla, A. Valibeygi, and R. A. de Callafon, "Microgrid dynamic modeling and islanding control with synchrophasor data," *IEEE Trans. Smart Grid*, vol. 11, no. 1, pp. 905–915, jan 2020.
- [8] F. M. Uriarte, C. Smith, S. Vanbroekhoven, and R. E. Hebner, "Micro-grid ramp rates and the inertial stability margin," *IEEE Trans. Power Syst.*, vol. 30, no. 6, pp. 3209–3216, 2015.
- [9] H. Bevrani, F. Habibi, P. Babahajyani, M. Watanabe, and Y. Mitani, "Intelligent frequency control in an AC microgrid: Online PSO-based fuzzy tuning approach," *IEEE Trans. Smart Grid*, vol. 3, no. 4, pp. 1935–1944, 2012.
- [10] I. Serban and C. Marinescu, "Control strategy of three-phase battery energy storage systems for frequency support in microgrids and with uninterrupted supply of local loads," *IEEE Trans. Power Electron.*, vol. 29, no. 9, pp. 5010–5020, 2014.
- [11] Y. Han, P. M. Young, A. Jain, and D. Zimmerle, "Robust control for microgrid frequency deviation reduction with attached storage system," *IEEE Trans. Smart Grid*, vol. 6, no. 2, pp. 557–565, 2015.
- [12] Z. Zhao, P. Yang, J. M. Guerrero, Z. Xu, and T. C. Green, "Multiple-time-scales hierarchical frequency stability control strategy of medium-voltage isolated microgrid," *IEEE Trans. Power Electron.*, vol. 31, no. 8, pp. 5974–5991, 2016.
- [13] Y. Zhang, A. M. Melin, S. M. Djouadi, M. M. Olama, and K. Tomsovic, "Provision for guaranteed inertial response in diesel-wind systems via model reference control," *IEEE Trans. Power Syst.*, vol. 33, no. 6, pp. 6557–6568, 2018.
- [14] J. Lopes, C. Moreira, and A. Madureira, "Defining control strategies for microgrids islanded operation," *IEEE Trans. Power Syst.*, vol. 21, no. 2, pp. 916–924, may 2006.
- [15] Y. Zhang, M. Olama, A. Melin, Y. Xue, S. Djouadi, and K. Tomsovic, "Synthesizing distributed energy resources in microgrids with temporal logic specifications," *2018 9th IEEE Int. Symp. Power Electron. Distrib. Gener. Syst. PEDG 2018*, 2018.
- [16] S. Wang and K. Tomsovic, "A novel active power control framework for wind turbine generators to improve frequency response," *IEEE Trans. Power Syst.*, vol. 33, no. 6, pp. 6579–6589, 2018.
- [17] —, "Fast frequency support from wind turbine generators with auxiliary dynamic demand control," *IEEE Trans. Power Syst.*, vol. 34, no. 5, pp. 3340–3348, 2019.
- [18] A. Gholami and A. Sun, "Towards resilient operation of multi-microgrids: an MISOPC-based frequency-constrained approach," *IEEE Trans. Control Netw. Syst.*, vol. PP, no. c, p. 1, 2018.
- [19] Y. Zhang, M. E. Raoufat, K. Tomsovic, and S. M. Djouadi, "Set theory-based safety supervisory control for wind turbines to ensure adequate frequency response," *IEEE Trans. Power Syst.*, vol. 34, no. 1, pp. 680–692, 2019.
- [20] Q. Shi, F. Li, and H. Cui, "Analytical method to aggregate multi-machine SFR model with applications in power system dynamic studies," *IEEE Trans. Power Syst.*, vol. 33, no. 6, pp. 6355–6367, 2018.
- [21] Y. Zhang, Y. Li, K. Tomsovic, S. Djouadi, and M. Yue, "Review on set-theoretic methods for safety verification and control of power system," *IET Energy Syst. Integr.*, 2020, early access.
- [22] A. Girard, "Reachability of uncertain linear systems using zonotopes," *Lect. Notes Comput. Sci.*, vol. 3414, pp. 291–305, 2005.
- [23] A. Girard, C. Le Guernic, and O. Maler, "Efficient computation of reachable sets of linear time-invariant systems with inputs," *Lect. Notes Comput. Sci. (including Subser. Lect. Notes Artif. Intell. Lect. Notes Bioinformatics)*, vol. 3927 LNCS, pp. 257–271, 2006.
- [24] M. Althoff, O. Stursberg, and M. Buss, "Reachability analysis of linear systems with uncertain parameters and inputs," *Proc. IEEE Conf. Decis. Control*, no. 0, pp. 726–732, 2007.
- [25] —, "Reachability analysis of nonlinear systems with uncertain parameters using conservative linearization," *Proc. IEEE Conf. Decis. Control*, pp. 4042–4048, 2008.
- [26] M. Althoff and B. H. Krogh, "Reachability analysis of nonlinear differential-algebraic systems," *IEEE Trans. Automat. Contr.*, vol. 59, no. 2, pp. 371–383, 2014.
- [27] L. Jaulin, M. Kieffer, and O. Didrit, *Applied Interval Analysis*. New York, NY, USA: Springer, 2006.
- [28] R. E. Moore, R. B. Kearfott, and M. J. Cloud, *Introduction to Interval Analysis*. Philadelphia, PA, USA: SIAM, 2009.
- [29] A. Ben-Tal, L. E. Ghaoui, and A. Nemirovski, *Robust Optimization*. Princeton, NJ, USA: Princeton University Press, 2009.
- [30] J. Löfberg, "Minimax approaches to robust model predictive control," Ph.D. dissertation, Linköping University, Linköping, Sweden, 2003.
- [31] D. Bertsimas and A. Thiele, "A robust optimization approach to inventory theory," *Oper. Res.*, vol. 54, no. 1, pp. 150–168, 2006.
- [32] J. Löfberg, "YALMIP: A toolbox for modeling and optimization in MATLAB," in *Proc. IEEE CCA/ISIC/CACSD Conf.*, Taipei, Taiwan, 2004. [Online]. Available: <http://users.isy.liu.se/johanli/yalmip/>